JOURNAL OF OPTOELECTRONICS AND ADVANCED MATERIALS Vol. 10, No. 6, June 2008, p. 1390 - 1395

Dependence of nickel ferrite EMR absorption coefficient on the method of preparation

A.S. NIKOLIĆ, P. OSMOKROVIĆ[* a,b], D. MANOJLOVIĆ, N. ŠOJIĆ[c], M.B. PAVLOVIĆ[b]
Faculty of Chemistry, Studentski trg 12-16, Belgrade, Serbia
[a]*Faculty of Electrical Engineering, B. Kralja Aleksandra 73, Belgrade, Serbia*
[b]*Department of Physics, Ruzveltova 1a, Belgrade, Serbia*
[c]*Groupe NanoSystèmes Analytiques Institut des Sciences Moléculaires - UMR 5255 CNRS, Université Bordeaux 1 – ENSCPB 16, Avenue Pey-Berland 33607 PESSAC Cedex FRANCE*

Nickel ferrites are among the most abundant members of the soft magnetic materials. In the last few decades, the interest for new methods of their preparation has increased, due to the fact that physical and chemical properties of these materials depend strongly on preparation conditions. In this paper, samples of $NiFe_2O_4$ were synthesized by standard sintering and via a chemical procedure from complex compounds with acetylacetonato ligands. Formation of the $NiFe_2O_4$ spinel phase was monitored by SEM, TEM, and XRD measurements. Average particle size was 20x20x4 nm (slabs). Masurements of the real and imaginary parts of permittivity and permeability were conducted on the obtained nickel ferrite samples in the 7-12 GHz frequency range. In addition to this, the electromegnetic radiation (EMR) absorption coefficient was calculated for all samples, using the Nicolson-Ross analysis. Examination of the obtained results lead to the conclusion that the method of synthesis, as well as final particle size, influence the EMR absorption coefficient in the observed frequency range.

(Received February 24, 2008, after revision March 31, 2008; accepted June 4, 2008)

Keywords: Nanocrystalline materials, Ferrites, Absorbers, Sintering, Nicolson-Ross analysis

1. Introduction

Magnetic nanoparticles possess unique physical properties as a consequence of dimensional reduction. Properties of nanoparticle materials, such as the coercive field, the Curie temperature, saturation magnetization, or absorption of incident electromagnetic radiation, can differ largely from bulk materials. Below a certain critical dimension, magnetic particles become a single domain and show superparamagnetic behaviour [1,2,3].

Microstructure is vital for material's magnetic properties, but its influence on these properties is poorly understood. From the technical point of view, magnetic characteristics of materials crucially depend on their microstructure [4]. A similar situation exists in conventional transition metal magnets, where control of microstructure is the central task in development of alloy systems with desirable technical properties (coercivity, remanence and permeability). Modern advances in both instrumentation and data analysis facilitate systematic size-strain crystallographic studies, which in conjunction with measurements of magnetic properties and of the absorption of incident electromagnetic radiation provide a better understanding of nanomagnetism. To the best of our knowledge, a systematic study of the relation between microstructure and absorption of incident electromagnetic radiation in nanoparticle materials has not been conducted so far. This has been one of the goals of this paper.

Cubic nanosize spinel ferrites (soft ferrites), with the general formula MFe_2O_4, are a class of well known magnetic materials, significant in applications such as high density information storage media, drug delivery, medical diagnostics, ferrofluids, electronic devices, catalysts, etc. [5,6]. Nano-scale ferrites are also a current topic of basic research in nanomagnetism. In the unit cell of spinels, oxygen ions form close packing, with M^{2+} and Fe^{3+} ions distributed between tetrahedral A (8a) and octahedral B (16d) interstitial sites. In most cases, ferrites with a spinel structure have $(M,Fe)_3O_4$ stoichiometry, where the cation/anion ratio is 3:4, although deviation from this stoichiometry is possible [7,8]. In cation deficit spinels, the vacancies present lead to modification of cation valence, thus influencing the physical properties.

Radar absorbing materials (RAMs) are intended to reduce the scattered signal by absorbing some part of the incident radiation. Microwave energy is converted into heat with hardly any noticeable temperature rise, since the energies involved are extremely small. Various kinds of materials can be made to absorb microwave energy by impregnating them with conducting materials, such as carbon and iron. RAMs can be employed to reduce radar signals from ships, ground military equipment, as well as at military facilities.

There are generally two types of materials used as absorbers: dielectric and magnetic RAMs. Adding carbon to an insulating material changes its electrical properties. Hence, carbon-based absorbers are called dielectric RAMs. The most familiar example of a dielectric RAM is found in anechoic chambers. Dielectric RAMs are usually too bulky and fragile, which makes them unsuitable for applications with limited space or severe mechanical conditions. Magnetic RAMs use iron compounds, such as

carbonyl iron and iron oxides (i.e. ferrites). Iron is efficient in dissipating radar waves and has been used in paints. It is quite effective against high-frequency radars used in moderns fighters. Unlike dielectric RAMs, magnetic RAMs are compact, thin and strong enough to withstand loads in a harsh environment. On the other hand, magnetic RAMs are heavy, expensive and their performance deteriorates as working temperature approaches the Curie point (in the range from 530 K to 800 K). They are, nonetheless, suitable for Mach 2 aircrafts. The materials have been embedded in a form of rubber tile, which can then be glued into a desired position. If used for aircrafts, coatings must be able to stay intact and attached to the plane surfaces during flight. Some parts of an aircraft, such as those around the jet pipe, experience high temperatures and the absorbers have to be made of ceramic-based RAMs.

The concept of absorbing incident electromagnetic radiation by intercepting the wave by an absorbing material is well known. The applications of this concept are numerous, particularly at microwave frequencies, including the use of absorbent coatings on the walls of anechoic chambers, as well as on exterior surfaces of military aircraft and vehicles to achieve radar invisibility [9]. When there is plenty of space available sufficient absorption of power over a wide bandwidth can generally be obtained by increasing the volume of the material and shaping its geometry. When the space is limited, which is the usual situation for most military applications, ensuring optimal bandwidth and reflectivity properties is a difficult design problem. Electromagnetic reflectivity over a frequency range, together with the weight, depth, cost, and durability of the material, determine the effectiveness of a specific absorber.

A thin coating of material can be theoretically modeled to give any desired reflectivity over a specified bandwidth, but practical realization of the material meets with severe constraints at microwave frequencies. Ideally, the designer wants to have control over material's permittivity, permeability and loss tangent values, but the main problem is related to the dearth of material with relative permeability significantly greater than unity ($\mu_r >> 1$) at frequencies in the microwave region. A class of materials, soft and hexagonal ferrites, having significant permeability values over very narrow frequency ranges, have been reported [10,11,12], but it is not yet obvious how to deploy these materials in order to obtain broadband absorption characteristics.

Measurement of complex permitivity ε_r and permeability μ_r, both vector quantities of dielectric or absorbing materials, has gained increasing importance with expanding use of the RF and microwave spectrum. If an absorber of electromagnetic radiation is to be efficient, the material must not only attenuate EM waves penetrating its volume, but must also present a good match to the incident waves at the air/material interface. Good absorption is provided with the real parts of permitivity and permeability (ε_r', μ_r') as well as the loss tangents ($\tan\delta_\mu$, $\tan\delta_\varepsilon$) being as large as possible, while good matching at the interface requires $\mu_r' = \varepsilon_r'$ and $\tan\delta_\mu = \tan\delta_\varepsilon$ [13].

This paper describes the influence of two different preparation methods for obtaining nickel ferrites ($NiFe_2O_4$) on the EMR absorption coefficient in the 7-12 GHz frequency range. One of the preparation methods is a novel chemical route for obtaining ultrafine nickel ferrites by using complexes with acetylacetonato ligands as precursors, while the other method is the standard sintering procedure. Structural and microstructural properties of ferrite samples obtained in these two ways are investigated using X-Ray Diffraction (XRD), Scanning Electron Microscopy (SEM), Transmission Electron Microscope (TEM). Masurements of the real and imaginary parts of permittivity (ε_r', ε_r'') and permeability (μ_r', μ_r'') were conducted on the obtained nickel ferrite samples in the 7-12 GHz frequency range. The ability of ferrite samples to absorb incident electromagnetic radiation is probed using Nicolson-Ross Analysis of EMR absorption coefficients.

2. The experiment

Powder samples of soft ferrites ($NiFe_2O_4$) were synthesized by standard sintering procedure (type 1 samples, made in Ei Ferrite, Belgrade) and by chemical procedure from complex compounds with acetylacetonato ligands (type 2 samples) [14-18].

For preparing the ultra fine powders (type 2 samples) of nickel ferrites at a relatively low temperature the method based on thermal decomposition of stoichiometric mixtures of Ni(II) and Fe(III) complexes with acetylacetonato- (2,4-pentadione) ligands was used [19]. Thermal decomposition was carried out with a heating rate of 10°C/min. The cooling rate was 20°C/min. Nanometric powders were obtained at low temperature (500°C). Thermal decomposition of Ni- and Fe-acetylacetonates enables the nucleation of elementary nickel ferrite cells, and their growth during the process differs from the classical sintering process, where diffusion between NiO and hematite crystals 1-2 μm in size takes place, and where the final size of particles is larger than the size of crystals in basic components. The average particle size for standard sintering method is several microns (μm), while the average particle size of thermal decomposition products is 10-15 nm, giving the size ratio of about 100:1.

The morphology of the obtained powders and the sizes of nickel ferrite crystallites were examined by Scanning Electron Microscopy SEM (JEOL JSM-5200) (prior to SEM surveys the crystals were gold sputtered in JFC 1100 ionic sputter coater) and with a combined field-emission (scanning) transmission electron microscope TEM (the grid was dried overnight at room temperature and observed with a FEI Tecnai Biotwin (120kV); prior to TEM investigations the powders were crushed in a mortar,

dispersed in ethanol, and fixed on a copper-supported carbon film). X-Ray Diffraction Analysis of the powders was performed by a Philips PW 1730 automatic diffractometer with CuKα graphite-monochrom radiation (λ = 0.1542 nm).

Measuring aparatus consists of a waveguide resonant cavity of special design and the HP8510B Network Analyzer. Disassembled cavity is shown in Fig. 1. It consists of a fixed short, mobile short and of several waveguide frames. On one of the frames two capacitive probes are mounted. Samples have been prepared by pressing the powder into the one of aluminium holders (27x27 mm frames) without thermal treatment. One frame has contained the sample powder, while other frames have remained empty. The transfer function between probes has been measured with the Network Analyzer. This function has a distinct maximum at the cavity resonant frequency. The width of the maximum depends on the Q-factor of the resonator i.e. on its overall losses.

The first step during the measurements is the calibration of the resonator, in order to find the electrical position of the mobile short. This is done by using the cavity with the frames without the sample. The equivalent circuit of the cavity is shown in Fig. 2. Connections in this circuit (with characteristic impedance equal to wave impedance of the dominant wave in the waveguide Z_v) represent the corresponding sections of the waveguide. Short connections are represented by impedances which include losses (Z_m). Probes are modeled by capacitors, while the generator and the resistors represent the Network Analyzer. For one measurement frequency, cavity resonance is achieved by moving the mobile short and noting the position of the pointer. This procedure is repeated for every frequency used in measurements.

In the next step, the cavity is assembled so that the frame with the sample is positioned at the fixed short (Fig. 3). Characteristic impedance of the section of waveguide with the sample is Z_d. The presence of the material of the sample changes electric and magnetic properties of the medium in one part of the resonator. This leads to the change of resonance frequency and produces losses. At the short, electric field in the waveguide approaches zero. Therefore, if the sample is thin, in this position the magnetic properties of the sample are dominant. For every frequency, resonance is achieved using the mobile short and readings are made of the position of the pointer and of the width of the resonance curve.

In the third step, the frame with the sample is positioned between the frame with probes and the mobile short (Fig. 4). In this position the sample affects the electric and magnetic fields. By tuning, resonanse is again established and readings are made of the position of the mobile short and of the resonance curve width.

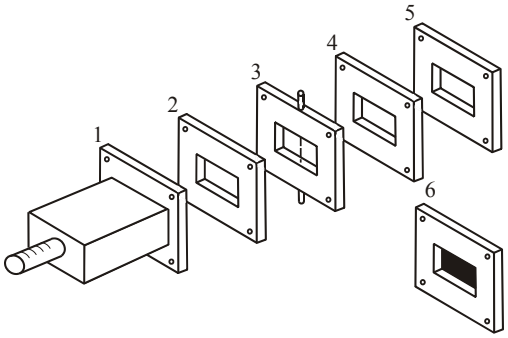

Fig 1. Disassembled cavity (1 - mobile short, 2- frame, 3 - frame with probes, 4 - frame, 5 - fixed short, 6 - frame with a sample).

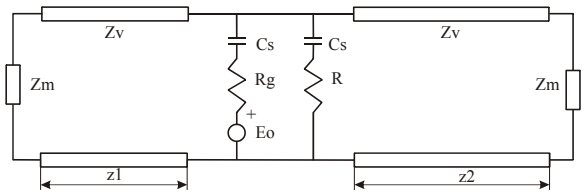

Fig 2. Equivalent circuit of the cavity with frames and with no sample.

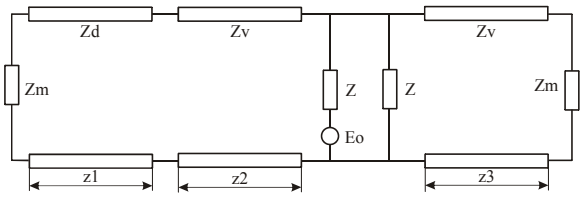

Fig 3. Equivalent circuit of the cavity assembled so that the frame with the sample is positioned at the fixed short.

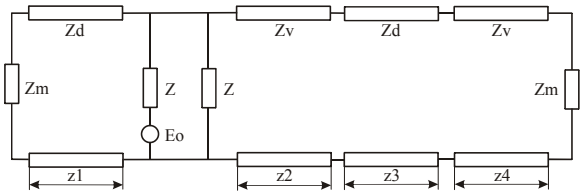

Fig. 4. Equivalent circuit of the cavity assembled so that the frame with the sample is positioned between the frame with probes and the mobile short.

In the last step, results are processed by the computer. Using Tuchstone software, the model of the waveguide is analyzed for each of the configurations (Figs. 2, 3 and 4). The parameters of the material (ε_r', ε_r'', μ_r', μ_r'') are optimized so that the resonant frequency of the cavity and the width of resonance curve coincide with measurement results.

3. Results and discussion

The basic structure of spinel ferrite is MFe_2O_4, where M denotes divalent metal ion (in this case Ni^{2+}). In a unit cell of spinel lattice there are eight tetrahedral and sixteen octahedral sites occupied by metal ions, or 1 tetrahedral and 2 octahedral for each formula unit. In the case of nickel ferrite eight units of $NiFe_2O_4$ go into a unit cell of the spinel structure. The ferric ions occupied the tetrahedral sites, but there is room for only half of them (eight). The remaining eight are sited on the octahedral sites, as do the eight Ni^{2+} ions.

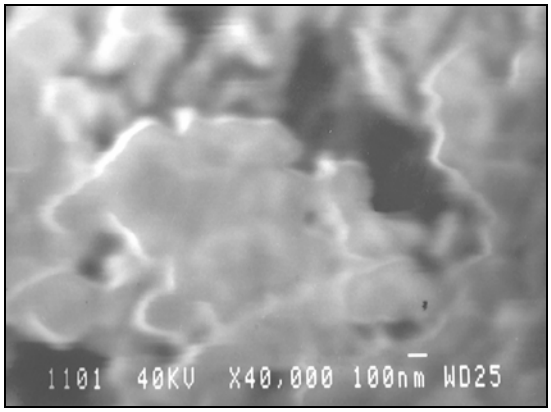

Fig. 5. SEM micrograph of nanoscale $NiFe_2O_4$ for samples prepared from complex compounds with acetylacetonato ligands.

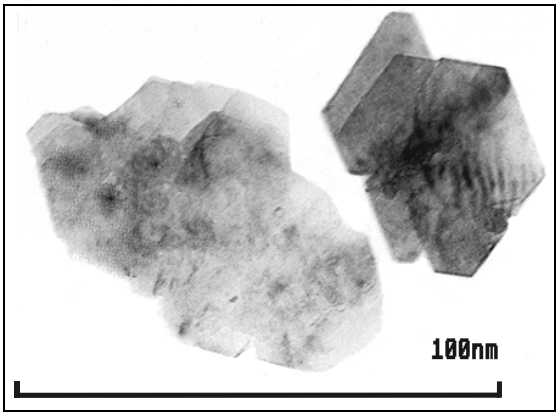

Fig. 6. TEM micrograph of nanoscale $NiFe_2O_4$ for samples prepared from complex compounds with acetylacetonato ligands.

Results obtained by electron microscopy show that type 2 samples, prepared from complex compounds with acetylacetonato ligands, are ultrafine with particle sizes in agreement with prevously reported values [16]. SEM micrographs for type 2 samples (Fig. 5) show that the nanoscale crystallites tend to agglomerate because of the dipolar feild of each crystallite. Agglomerated crystallites form grains with sizes up to 250 nm. TEM micrographs for type 2 samples (Fig. 6) show that the nanoscale crystallite form grains with sizes 20x20x4 nm (slabs), consistent with the average crystallite size determined by XRD. X-ray analysis (Fig. 7) shows no peaks of the starting compound and only the full spectrum of $NiFe_2O_4$ characteristic peaks is present in the pattern.

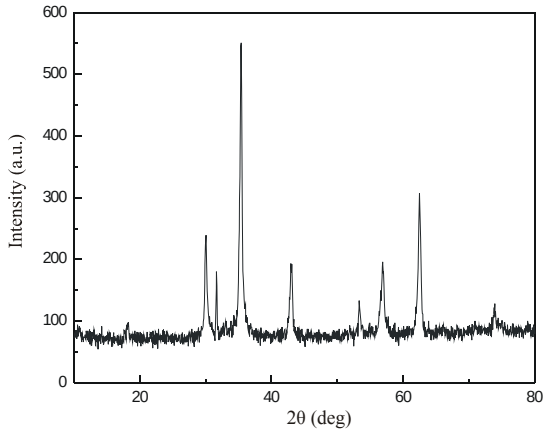

Fig. 7. XRD patterns of $NiFe_2O_4$ for samples prepared from complex compounds with acetylacetonato ligands.

As a first approximation, crystallite sizes of powders were calculated by means of the Scherrer equation, using XRD data, as:

$$S = 0.9\lambda/(B\cos\theta_B) \tag{1}$$

where S is the crystallite grain size, λ is the wavelength of the X-ray source, θ_B is the Bragg angle of the considered XRD peaks, and B represents the FWHM line broadening obtained as follows:

$$B^2 = B_m^2 - B_s^2 \tag{2}$$

where B_m is the FWHM line broadening of the material and B_s represents the FWHM line broadening of the internal standard (α-Al_2O_3). The resulting value of the crystallite size, obtained from the (111) strongest reflections, is 12 nm.

Complex permittivity and permeability of ferrite samples obtained in both ways (types 1 and 2) were obtained from measurements conducted with the HP 8510 Network Analyzer system. From the obtained frequency dependence of permittivity and permeability the EMR attenuation coefficient α was calculated using the formula:

$$\alpha = 2\pi f\sqrt{\mu_0\varepsilon_0}\sqrt{\varepsilon_r'\mu_r'/2}\cdot \sqrt{\left(\tan\delta_\mu\tan\delta_\varepsilon - 1\right) + \left(1 + \tan^2\delta_\mu\tan^2\delta_\varepsilon + \tan^2\delta_\mu + \tan^2\delta_\varepsilon\right)^{1/2}} \tag{3}$$

where the loss tangents are defined by $\tan\delta_\mu = \mu_r''/\mu_r'$ and $\tan\delta_\varepsilon = \varepsilon_r''/\varepsilon_r'$ (μ_r' and ε_r' being the real parts, and μ_r'' and ε_r'' the imaginary parts of permeability and permittivity, respectively).

Permittivity real and complex parts exhibit frequency dependence in both type 1 and type 2 samples, and yet without any marked maxima, so that both examined materials could be used as wide-range absorbents. Type 1 samples exhibit higher values of both the real and the imaginary part of permittivity than those of type 2 samples (Fig. 8). On the other hand, type 2 samples exhibit higher values of both the real and the imaginary part of permeability (Fig. 9).

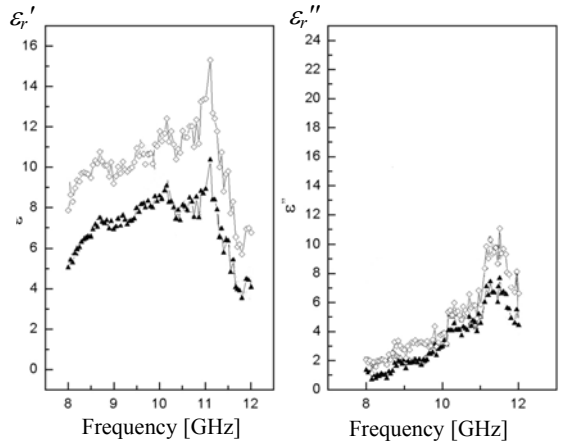

Fig. 8. Values of the real (ε_r') and the imaginary part (ε_r'') of permittivity for nickel ferrite samples ◇ - obtained by standard sintering and ▲ - obtained by chemical procedure from complex compounds with acetylacetonato ligands.

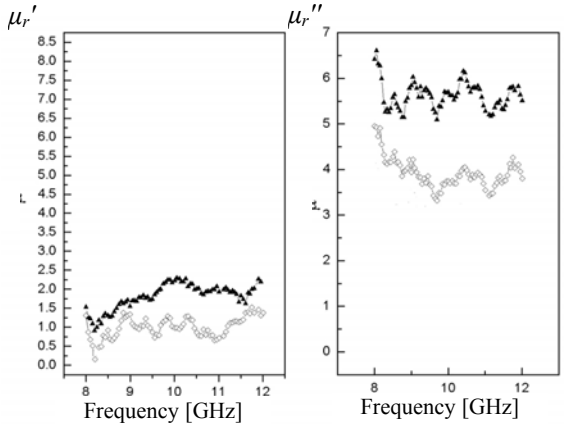

Fig. 9. Values of the real (μ_r') and the imaginary part (μ_r'') of permeability for nickel ferrite samples ◇ - obtained by standard sintering and ▲ - obtained by chemical procedure from complex compounds with acetylacetonato ligands.

Values of EMR attenuation coefficient (α) calculated from expression (3) are presented in Fig. 10, in linear (Fig. 10a) and log scale (Fig. 10b). It may be concluded that EMR attenuation coefficient depends on the method of preparation. Higher values of EMR attenuation coefficient observed in type 1 samples, obtained by standard sintering, are a result of the granule-weight to granule-surface ratio, as well as of the large number of dislocations and impurities in the crystal structure concentrated at granule surfaces. Lower values of EMR attenuation coefficient observed in type 2 samples, obtained by chemical procedure from complex compounds with acetylacetonato ligands, could be a result of the perfect packing of the crystal structure at crystallite surfaces, as well as of the low number of dislocations, even with the much smaller volume of the crystallites in these samples.

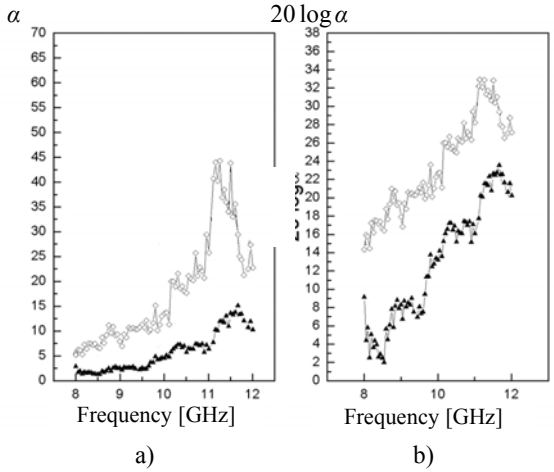

Fig. 10. Values of EMR attenuation coefficient (α) for nickel ferrite samples ◇ - obtained by standard sintering and ▲ - obtained by chemical procedure from complex compounds with acetylacetonato ligands, presented in a) linear and b) logarithmic scale.

4. Conclusions

Based on the obtained results it can be concluded that nickel ferrite ($NiFe_2O_4$) produced by the standard sintering method gives better results in regard to EMR attenuation than does nickel ferrite obtained by chemical procedure from complex compounds with acetylacetonato ligands. For nickel ferrite samples obtained by standard sintering EMR attenuation coefficient has a practically constant value (roughly between 10 and 30 dB) over the whole frequency range observed in this paper (7-12 GHz), which ranks these soft ferrites among the most favourable wide-range radar absorbents. The configuration of the soft ferrites obtained by this method is a single-layer one, as opposed to complex multi-layer configurations applied so far [13]. Further investigation of the synthesis of soft ferrites with different chemical compositions (e.g. $MnMgFe_2O_4$), based on Fe^{+3} ion replacement by other trivalent ions (Al, Y, Cr^{+3}…), as well as the mixing of soft ferrites with weak isolators, may lead to even better results. Final judgement on the applicability of these

materials for wide-range radar absorbers demands an extension of the investigated frequency range toward higher frequencies.

Acknowledgment

Participation of P. Osmokrović and M.B. Pavlović on this work is supported by the Ministry of Science and Environmental Protection of the Republic of Serbia under contract 141046.

References

[1] R. H. Kodoma, A. E. Berkowitz, E. J. McNiff, S. Foner., Phys. Rev. Lett. **77**, 394 (1996).
[2] R. H. Kodoma, J. Magn. Magn. Mat. **200**, 359 (1999).
[3] E. Tronc et al. J. Magn. Magn. Mat. **262** (2003).
[4] J. F. Herbst Rev. Mod. Phys. **63**, 819 (1991).
[5] A. A. Novakova, V. Yu. Lanchinskaya, A. V. Volkov, T. S. Gendler, T. Yu. Kiseleva, M. A. Moskvina, S. B. Zezin, J. Magn. Magn. Mat. **258-259**, 354 (2003).
[6] C. R. Vestal, Z. Chang J Chem. Mat. **14**, 3817 (2002)
[7] J. Topfer, L. Liu, R. Dieckmann, Solid State Ionic **159**, 397 (2003).
[8] B. Antic, A. Kremenovic, A. S. Nikolic, M. Stoiljkovic J. Phys. Chem. **B108** 12646 (2004).
[9] W. H. Emerson, IEEE Trans on Antennas and Propagation, AP-21, (4) 484 (1973).
[10] H. Severin, P. J. Stoll, Z. Angew. Phys. **23**(3), 209 (1967).
[11] C. Heck, "Magnetic Materials and their Applications", p. 345 Butterworths, London, (1974).
[12] R. S. Tabble, D. J. Craik, "Magnetic Materials" p.407 Wiley-Interscience, New York, (1969).
[13] M. B. Amin, J. R. James, Radio and Electronic Engineer **51**(5), 209 (1981).
[14] A. S. Nikolić, B. Antić, M. B. Pavlović, D. Rodić, Proc.Nat. Sci., 211 (1994).
[15] S. Djurić, P. M. Nikolić, Z. B. Maričić,V. Blagojević, O. S. Aleksić, M. B. Pavlović, J. Pavlović, Proc. XXXIII ETAN Conference, Novi Sad, Yugoslavia, 27 (1989).
[16] A. S. Nikolić, N. Cvetković, S. Đurić, J. Puzović, M. B. Pavlović, Mater. Sci. For. 199 (1998).
[17] I. Nicolaescu, J. Optoelectron. Adv. Mater. **8,** 333 (2006).
[18] E. Manova, B. Kunev, D. Paneva, I. Mitov, L. Petrov, C. Estournés, C. D'Orléans, J.-L. Rehspringer, M. Kurmoo, Chem Mater. **16**, 5689 (2004).
[19] A. S. Nikolić, Z. B. Maričić, T. J. Sabo, M. Kuraica, S. Djurić, N. Juranić, J. Serb. Chem.. Soc. 297 (1999).

*Corresponding author: opredrag@verat.net